BMB
Reports

BMB Rep. 2025; 58(6): 244-249
www.bmbreports.org

High-resolution detection of *RPS24* microexon variations reveals novel splicing patterns in response to *KRAS*-targeted therapy in lung adenocarcinoma

Dahye Nam[1], *Bin Tian*[2], *Jiyeon Park*[3,*] *& Yeun-Jun Chung*[1,3,*]

[1]Department of Microbiology, College of Medicine, The Catholic University of Korea, Seoul 06591, [2]Genome Regulation and Cell Signaling Program, The Wistar Institute, Philadelphia, PA 19104, USA, [3]Precision Medicine Research Center, College of Medicine, The Catholic University of Korea, Seoul 06591, Korea

Alternative splicing (AS) dysregulation is increasingly recognized as a critical factor in cancer progression and drug response. However, precisely detecting and characterizing complex splicing events, particularly those involving microexons, remains technically challenging. Ribosomal Protein 24 (*RPS24*), which contains three microexons (3, 18, and 22 bp), serves as an ideal model for studying complex AS regulation in cancer. We developed a high-resolution detection method for *RPS24* microexon variations and investigate their relationship with *KRAS* proto-oncogene, GTPase (*KRAS*) inhibition in lung adenocarcinoma (LUAD) to identify potential biomarkers for *KRAS*-targeted inhibitors. We established an integrated methodological approach combining RNA-seq analysis with fragment analysis to detect *RPS24* AS patterns. Using this method, we analyzed *RPS24* AS across a panel of lung cancer cell lines and examined AS changes in *KRAS*-mutant cell lines following treatment with *KRAS* inhibitors. Our method successfully characterized distinct *RPS24* AS isoform compositions across lung cancer cell lines, demonstrating high accuracy in detecting 3 bp variations. In *KRAS*-mutant cell lines, we observed a consistent upregulation of the 3 bp-containing isoform following *KRAS* inhibition, indicating a specific correlation with treatment response. This study provides a robust methodology for analyzing complex AS events and supports the *RPS24* 3 bp-containing isoform as a potential biomarker for *KRAS* inhibitor response in LUAD. These findings offer new insights into the molecular mechanisms of *KRAS* inhibitor therapy and strategies for monitoring treatment response. [BMB Reports 2025; 58(6): 244-249]

*Corresponding authors. Yeun-Jun Chung, Tel: +82-2-2258-7343; Fax: +82-2-537-0572; E-mail: yejun@catholic.ac.kr; Jiyeon Park, Tel: +82-2-3147-9008; Fax: +82-2-537-0572; E-mail: parkji7@gmail.com

https://doi.org/10.5483/BMBRep.2025-0026

Received 28 February 2025, Revised 11 April 2025, Accepted 19 April 2025, Published online 10 June 2025

Keywords: Alternative splicing, *KRAS*, Lung cancer, *RPS24*

INTRODUCTION

Alternative splicing (AS) is a crucial regulatory mechanism in eukaryotes that generates diverse mRNA isoforms from a single gene. Recent pan-cancer transcriptomic analyses have revealed that tumor samples exhibit up to 30% more AS events than normal tissues (1). These AS patterns often produce cancer-associated oncogenic isoforms that influence key hallmarks of cancer, including cell proliferation, apoptosis, metabolism, invasion, angiogenesis, and metastasis (2, 3). Although understanding these AS events is essential for developing new therapeutic strategies, accurately detecting and characterizing complex AS events, particularly those involving microexons, remains technically challenging (4).

Lung adenocarcinoma (LUAD) remains one of the most lethal cancer types, with treatment strategies increasingly guided by specific mutation profiles (5). While targeted therapies have been successfully developed for epidermal growth factor receptor (EGFR) mutations, *KRAS* mutations present greater therapeutic challenges. Although *KRAS* was long considered "undruggable," recent breakthroughs have led to the approval of *KRAS* G12C-specific inhibitors, including sotorasib and adagrasib (6, 7). However, major challenges remain, including the need for therapeutics targeting other common variants (G12D, G12V) and strategies to overcome acquired drug resistance. While *KRAS* G12C inhibitors have demonstrated clinical efficacy, response rates vary widely, and resistance frequently emerges within months of treatment initiation (8, 9). This underscores the urgent need for reliable biomarkers to predict treatment response and resistance.

The ribosomal protein S24 (*RPS24*) gene, which contains three microexons (3, 18, and 22 bp), serves as an ideal model for studying complex AS regulation, particularly at the 3′ splice site connecting to exon 4. *RPS24* AS patterns exhibit tissue and spatial specificity (10) and have been linked to various cellular processes, including hypoxia and autophagy (11, 12). Our previous study identified correlations between epithelial-mesenchymal transition (EMT) and specific *RPS24* AS patterns (13). However, the role of *RPS24* AS in lung cancer, particularly

ISSN: 1976-670X (electronic edition)

in *KRAS*-mutant contexts, remains poorly understood.

To address these challenges, we developed an integrated methodological approach combining RNA-seq and fragment analysis to detect *RPS24* AS changes with high resolution. Our study findings suggest that the *RPS24* 3 bp-inclusion isoform could serve as a potential biomarker for *KRAS*-targeted therapy in LUAD.

RESULTS

Analysis of splice junction reads as a suitable method for identifying AS isoforms within the *RPS24* microexons

AS of the *RPS24* gene generates multiple isoforms through the differential inclusion of three microexons (3 bp, 18 bp, and 22 bp) located between constitutive exons 4 and 6. Transcriptome analysis revealed multiple splice junctions between exon 4 and subsequent exons, which define the structural diversity of *RPS24* AS isoforms (Fig. 1A, top). To characterize these patterns, we quantified junction reads connecting exon 4 to downstream exons and calculated the relative proportion of each junction type per sample (Fig. 1B). Transcriptome data from 135 non-small cell lung cancer (NSCLC) cell lines in the cancer cell line encyclopedia (CCLE) database revealed distinct, cell line-specific splicing patterns (Fig. 1B). The ex4:22bp and ex4:ex6 junctions exhibited nearly ubiquitous expression, appearing in over 98% of cell lines. The ex4:3bp junction was expressed in 89 cell lines (66% of the total 135, using a >2% expression threshold), while the ex4:18bp junction, previously reported as muscle-specific, was detected in only one cell line (NCI-H2106).

Gene Set Enrichment Analysis (GSEA) identified biological pathways associated with *RPS24* AS patterns. The ex4:3bp junction, expressed in approximately half of the lung cancer cell lines, showed a significant positive correlation with oxidative

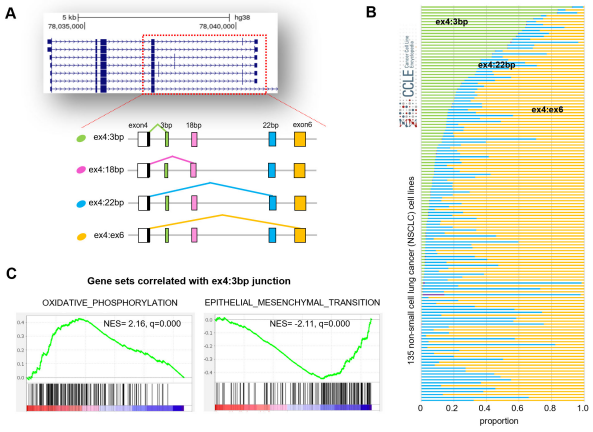

Fig. 1. Analysis of *RPS24* alternative splicing isoforms with three microexons in RNA sequencing data. (A) Classification of *RPS24* alternative splicing (AS) isoforms. The upper panel shows the *RPS24* transcript structure in the UCSC genome browser, highlighting three microexons located between exons 4 and 6 of the *RPS24* gene. The lower panel illustrates four distinct splicing patterns defined by junction reads between exon 4 and subsequent exons: ex4:3bp (green; exon 4 followed by a 3-bp microexon), ex4:18bp (pink; exon 4 followed by an 18-bp microexon), ex4:22bp (cyan; exon 4 followed by a 22-bp microexon), and ex4:ex6 (orange; direct splicing from exon 4 to exon 6). (B) Distribution of *RPS24* AS isoform proportions across 135 non-small cell lung cancer (NSCLC) cell lines. Each row represents a cell line, with colors indicating the relative proportion of each AS isoform, calculated based on junction reads originating from exon 4. (C) Gene Set Enrichment Analysis (GSEA) of pathways significantly correlated with ex4:3bp junction usage. Left: positive correlation with the oxidative phosphorylation pathway (NES = 2.16, q = 0.000). Right: negative correlation with epithelial-mesenchymal transition (NES = −2.11, q = 0.000). NES, Normalized enrichment score; q, adjusted P-value.

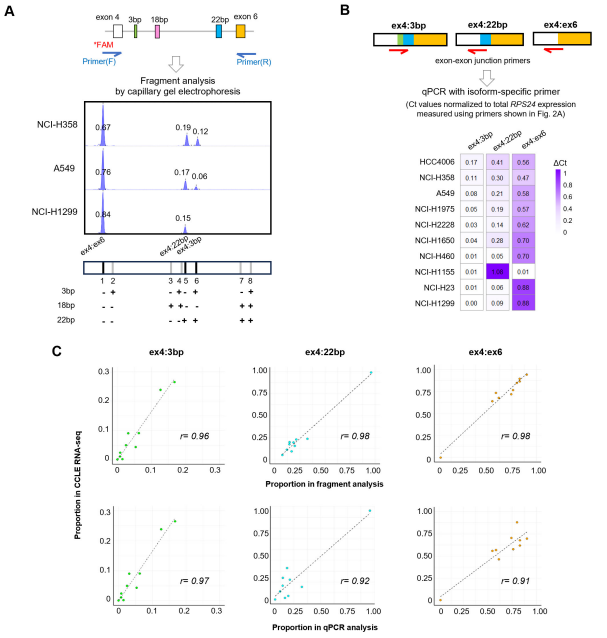

Fig. 2. Experimental validation of *RPS24* alternative splicing patterns in lung cancer cell lines. (A) Fragment analysis of *RPS24* AS isoforms. The upper panel shows the primer design strategy, with a fluorescently labeled forward primer (FAM) spanning exons 4 to 6. The lower panel presents representative electropherograms from fragment analysis of three cell lines (NCI-H358, A549, NCI-H1299), where each peak corresponds to a different *RPS24* AS isoform. Numbers above peaks indicate the relative proportions of each isoform, calculated from peak areas. The table below the electropherograms shows the presence (+) or absence (−) of each microexon in theoretical isoform combinations. Black lines represent detected isoforms, while gray lines indicate theoretical isoforms not observed in the sample. (B) Isoform-specific qPCR analysis. The upper panel shows the design of isoform-specific primers targeting distinct junction sequences. The lower heatmap displays delta Ct values for three major isoforms (ex4:3bp, ex4:22bp, and ex4:ex6) across ten selected lung cancer cell lines, using the primer set from panel A as a reference. (C) Correlation analysis between different quantification methods. Scatter plots depict correlations between junction read analysis from CCLE RNA-seq and fragment analysis (upper panels) or qPCR analysis (lower panels) for each isoform (ex4:3bp, ex4:22bp, and ex4:ex6). Pearson correlation coefficients (r) are indicated for each comparison. Dotted lines represent regression lines.

phosphorylation genes (normalized enrichment score [NES] = 2.16, adjusted P-value (q) = 0.000) and a negative correlation with epithelial-mesenchymal transition genes (NES = −2.11, adjusted P-value [q] = 0.000) (Fig. 1C, Supplementary Tables 1 and 2). The expression of the ex4:22bp junction showed significant positive correlation with E2F target genes (NES = 1.92, q = 0.002), while the ex4:ex6 junction showed significant correlation with immune-related genes such as those involved in inflammatory response (NES = 2.27, q = 0.000) (Supplementary Tables 3 and 5). Interestingly, consistent trend of association was observed between the three isoforms and *KRAS* signaling pathways, despite not reaching statistical significance ($q < 0.05$) (Supplementary Tables 1-6). These findings suggest a potential functional relationship between *RPS24* AS and *KRAS* pathway regulation that warrants further investigation.

Complex splicing patterns were validated using multiple approaches

To validate the specificity and quantitative accuracy of *RPS24* AS patterns, we employed complementary experimental approaches to analyze isoforms in ten selected lung cancer cell lines from the CCLE database. Given the presence of consecutive microexons, we performed fragment analysis using fluorescently labeled primers spanning exon 4 to exon 6, enabling single-nucleotide resolution separation and quantification via capillary electrophoresis (Fig. 2A). Although eight AS isoforms could theoretically arise from different microexon combinations, only three were detected in lung cancer cell lines. The 18 bp microexon was consistently absent, as indicated by the lack of peaks corresponding to positions 3, 4, 7, and 8. Additionally, the 3 bp microexon was invariably co-expressed with the 22 bp microexon (peak 6). The ex4:3bp junction represents an isoform containing both 3 bp and 22 bp microexons, the ex4:22bp junction corresponds to an isoform containing only the 22 bp microexon, and the ex4:ex6 junction identifies an isoform lacking all microexons.

For further validation, we performed isoform-specific quantitative polymerase chain reaction (qPCR) using junction-specific primers using 10 lung cancer cell lines (Fig. 2B). While distinguishing the ex4:3bp junction was challenging due to its minimal 3 bp difference from ex4:22bp, we successfully designed and validated specific primers via Sanger sequencing (data not shown). The quantitative results from fragment analysis and isoform-specific qPCR strongly correlated with RNA-seq data from the CCLE database ($r > 0.9$) (Fig. 2C), demonstrating the reliability and accuracy of our methodology for *RPS24* AS isoform identification and quantification.

KRAS signaling regulates *RPS24* alternative splicing in lung cancer cells

Based on GSEA identifying *KRAS* activation signatures associated with *RPS24* AS isoforms (Supplementary Table 1), we investigated the relationship between *KRAS* signaling and *RPS24* AS patterns using validated analytical methods. Experiments in *KRAS*-activated lung cancer cell lines NCI-H358 and A549 demonstrated that small interfering RNA (siRNA)-mediated *KRAS* knockdown significantly increased ex4:3bp expression by 1.3- and 3.3-fold, respectively (t-test, $P < 0.005$) (Fig. 3A, GSE198289). To further validate this relationship, we analyzed datasets from cells treated with *KRAS*- targeting therapeutics. Treatment with *KRAS* G12C inhibitors (sotorasib and adagrasib) consistently increased ex4:3bp expression in NCI-H358 cells harboring the G12C mutation (Fig. 3B, GSE229070 and GSE275534). Notably, this ex4:3bp upregulation was absent in sotorasib-resistant NCI-H358 cells, suggesting a potential link between this AS event and drug response. Additionally, in the NCI-H358 cells from another dataset (GSE103021), treatment with the downstream mitogen-activated protein kinase (MEK) 1/2 inhibitor (trametinib) and G12C-specific inhibitor (ARS-1620) also increased the ex4:3bp ratio with similar magnitude (Supplementary Fig. 1). In A549 cells, which carry the *KRAS* G12S mutation, treatment with trametinib similarly increased ex4:3bp expression in independent datasets (Fig. 3C, GSE89127 and GSE247512). All these results validate the regulation of ex4:3bp in response to *KRAS* signaling.

To identify potential upstream regulators of this AS event, we analyzed the expression patterns of 404 splicing-related genes across different *KRAS* pathway inhibition models (14). Differential gene expression across six datasets (fold change ≥ 1.2, $P < 0.05$ in all datasets) identified *PSEN1* as the only consistently upregulated gene, while 20 genes were consistently downregulated (Supplementary Fig. 2A). Among the downregulated genes, we identified two well-characterized splicing regulators, *SRSF2* and *SRSF7*. Analysis of an *SRSF2*-overexpressing A549 cell dataset revealed that *SRSF2* overexpression resulted in a 1.3-fold decrease in ex4:3bp expression (Supplementary Fig. 2B, GSE186872). These findings suggest a regulatory mechanism in which *KRAS* activation elevates *SRSF2* expression, leading to the suppression of the ex4:3bp *RPS24* isoform, establishing a functional link between *KRAS* signaling and *RPS24* AS.

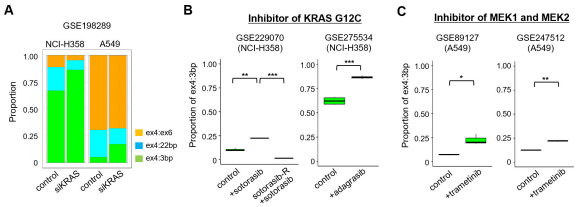

Fig. 3. *KRAS* signaling regulates *RPS24* alternative splicing. (A) Proportions of *RPS24* AS isoforms in NCI-H358 and A549 cells following *KRAS* knockdown (si*KRAS*) compared to the control (GSE198289). (B) Effects of *KRAS* G12C inhibitors on the ex4:3bp proportion. Left: NCI-H358 cells treated with sotorasib and its resistant derivative (GSE229070). Right: NCI-H358 cells treated with adagrasib (GSE 275534) (*$P < 0.05$, **$P < 0.005$, ***$P < 0.0005$). (C) Effects of MEK1/2 inhibitor (trametinib) treatment on the ex4:3bp proportion in A549 cells (GSE89127 and GSE247512).

Differential effects of sotorasib on *RPS24* splicing in lung cancer cells with distinct *KRAS* mutations

We examined the effects of *KRAS* inhibition on *RPS24* AS by assessing sotorasib treatment in two lung cancer cell lines with different *KRAS* mutations: NCI-H358 and A549. Cell viability analysis revealed distinct sensitivity patterns. NCI-H358 cells (*KRAS* G12C mutation) exhibited high sensitivity to sotorasib, with a marked reduction in viability at low concentrations (0.01-0.03 μM) (Fig. 4A, left). A549 cells (*KRAS* G12S mutation not directly targeted by sotorasib) showed decreased sensitivity, requiring higher concentrations (5-25 μM) to achieve similar reductions in viability (Fig. 4A, right). Based on these results, we selected sotorasib concentrations that maintained approximately 80% cell viability for further experiments (indicated by red dotted lines).

In NCI-H358 cells, fragment analysis demonstrated a 1.7-fold increase in ex4:3bp isoform ratios following treatment with 0.01 μM sotorasib ($P < 0.005$) (Fig. 4B, left and middle). Similarly, qPCR analysis confirmed a 1.7-fold increase in ex4:3bp isoform expression at the same concentration (Fig. 4B, right). In contrast, A549 cells showed no notable changes in ex4:3bp levels at either low (0.01 μM) or high (15 μM) concentrations (Fig. 4C, left and middle). The qPCR results aligned with those of the fragment analysis (Fig. 4C, right). These findings indicate that selective *KRAS* G12C inhibition by sotorasib modulates *RPS24* AS, enhancing ex4:3bp isoform expression specifically in mutation-matched cell lines.

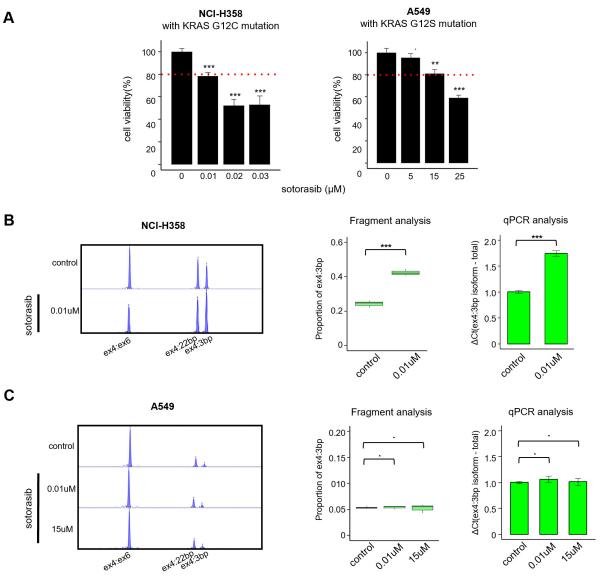

Fig. 4. Differential effects of sotorasib treatment on *RPS24* alternative splicing in *KRAS*-mutant lung cancer cell lines. (A) Cell viability assays showing differential sensitivity to sotorasib treatment in NCI-H358 cells with *KRAS* G12C mutation (left) and A549 cells with *KRAS* G12S mutation (right). Red dotted lines indicate the 80% cell viability threshold used for selecting treatment concentrations. Statistical significance compared to control: *$P < 0.05$, **$P < 0.005$, ***$P < 0.0005$. (B) *RPS24* AS analysis in NCI-H358 cells treated with sotorasib. The left panel shows representative electropherograms from fragment analysis, indicating relative proportions of each isoform after 3 days of sotorasib treatment at 0.01 μM. The middle and right panels show quantification of the ex4:3bp isoform using fragment analysis and qPCR analysis, respectively, after 3 days of treatment. (C) *RPS24* AS analysis in A549 cells treated with sotorasib. The left panel shows representative electropherograms from fragment analysis, indicating relative proportions of each isoform at both 0.01 μM and 15 μM concentrations. The middle and right panels show quantification of the ex4:3bp isoform using fragment analysis and qPCR analysis, respectively, after 3 days of treatment.

DISCUSSION

In this study, we present two key findings: the development of a methodology for complex AS analysis and the characterization of *RPS24* AS regulation in *KRAS*-activated lung cancer. First, we developed an effective approach for analyzing complex AS events involving three microexons in *RPS24*. Current splicing analysis tools struggle to model complex splicing events accurately, particularly the 3 bp microexon event identified in this study. Our junction read analysis method for RNA-seq data enabled efficient screening of large-scale transcriptome datasets, while fragment analysis proved highly effective for precise microexon AS detection. Fragment analysis also offers advantages in simplicity (requiring only PCR followed by capillary electrophoresis) and cost-effectiveness, making it particularly suitable for potential clinical applications. A key advantage of this method is that a single primer set can distinguish between isoforms differing by as little as 1 bp, eliminating the bias associated with isoform-specific PCR approaches.

Using this methodology, we investigated the role of *RPS24* AS in *KRAS*-activated cells. Our selection of *KRAS* LUAD models was informed by previous findings (13), which demonstrated dynamic *RPS24* AS changes during EMT in *KRAS*- activated A549 and NCI-H358 cells. While our prior study focused on the universally expressed ex4:22bp isoform, the present study revealed more pronounced changes in the ex4:3bp isoform specifically in *KRAS*-mutant models. Notably, only one-third of the lung cancer cell lines expressed the ex4:3bp isoform. We observed precise regulation of *RPS24* ex4:3bp in response to both siRNA-mediated *KRAS* inhibition and targeted therapeutics affecting *KRAS* protein levels and downstream signaling. Moreover, decreased ex4:3bp expression in drug-resistant cell lines suggests its potential as a biomarker for drug resistance. We also observed consistent downregulation of key splicing factors following *KRAS* inhibition and downstream signaling suppression. Overexpression studies of *SRSF2*, a well-established splicing regulator in lung cancer, further supported this association (15).

While our findings strongly support the relationship between *RPS24* ex4:3bp and *KRAS* signaling, the precise molecular mechanism remains unverified. Future isoform-specific knock-out and knock-in experiments are necessary to determine whether this isoform affects ribosome biogenesis or influences *RPS24*

protein-protein interactions. Such studies would provide crucial insights into the mechanistic role of *RPS24* AS in cancer development and progression.

In conclusion, our findings advance both the technical aspects of studying complex AS events and our understanding of the impact of *KRAS* signaling on ribosomal protein regulation through AS. This work opens new avenues for developing novel therapeutic strategies targeting these processes.

MATERIALS AND METHODS

Public data source

CCLE RNA-seq data were obtained from PRJNA523380 in the NCBI Sequence Read Archive (SRA). For other public RNA-seq datasets, sequencing files were downloaded from the SRA through a search on the Gene Expression Omnibus (GEO) website (https://www.ncbi.nlm.nih.gov/geo/). The raw data were in SRA file format, so they were converted to FASTQ files using the SRA Toolkit. The FASTQ files were mapped to the reference genome (hg38) using the STAR aligner in two-pass mode (16). Only the SJ.out.tab files summarizing splice junctions, one of the output files of STAR, were used.

RPS24 AS analysis using splice junction reads

For each dataset, splice junction reads were combined on a sample-by-sample basis, and reads spanning exon 4 of the *RPS24* gene were extracted. Exon 4 of *RPS24* is consistently expressed across all isoforms, with variations arising from subsequent exons. When no microexon exists between exon 4 and exon 6, the resulting isoform is denoted as "ex4:ex6." Other isoforms are classified as follows: if exon 4 is followed by a 3-bp microexon, the isoform is designated as "ex4:3bp"; if exon 4 is followed by an 18-bp microexon, the isoform is labeled as "ex4:18bp"; and if exon 4 is directly followed by a 22-bp microexon, the isoform is termed "ex4:22bp." For each individual sample within the dataset, the total count of junction reads originating from exon 4 was quantified to measure the overall expression level of the *RPS24* gene specifically within that sample. Additionally, to assess isoform proportions, the ratio was calculated by dividing the number of junction reads representing each isoform by the total number of junction reads originating from exon 4.

Gene expression analysis and gene set enrichment analysis

Gene expression analysis was performed using multiple data sources. For CCLE cancer cell lines, gene expression data were obtained through the DepMap R package, expressed in Transcripts Per Million (TPM) to facilitate cross-sample comparisons. For GEO datasets, raw sequencing reads were aligned to the human reference genome (hg38) using the STAR aligner, and gene expression levels were quantified using HTSeq 2.0 (17). Expression values were normalized using the trimmed mean of M values (TMM) method implemented in the edgeR package (18). To investigate splicing regulation, a curated set of 404 human RNA splicing-related genes from published literature was used (14). Pearson's correlation analysis was conducted to assess the relationships between *RPS24* alternative splicing isoforms and gene expression levels across cell lines. Correlation coefficients were calculated to identify potential regulatory interactions between splicing factors and *RPS24* isoform selection. Changes in splicing factor expression were visualized using the *pheatmap* R package, where log2 ratios relative to control conditions were hierarchically clustered into a heatmap. GSEA was performed to identify biological processes enriched in genes correlated with the inclusion rate of each *RPS24* AS isoform (19). Correlation coefficients between each isoform proportion and gene expression values were calculated and used as input for the GSEA pre-ranked test. For each isoform, positively and negatively correlated gene sets were identified, using Hallmark gene sets from the Human Molecular Signatures Database (MSigDB).

Cell lines and drug treatment

The NSCLC cell lines used in this experiment were purchased from the American Type Culture Collection and the Korea Cell Line Bank. The cell lines included A549, NCI-H358, NCI-H23, NCI-H460, NCI-H1155, NCI-H1975, NCI-H1650, HCC4006, NCI-H1299, and NCI-H2228. All cell lines were cultured in RPMI-1640 medium (HyClone, cat. SH30255.01) supplemented with 10% Fetal Bovine Serum (HyClone, cat. SH30919.03) and 1% Penicillin-Streptomycin (Thermo, cat. 15070063) at 37°C in a 5% CO_2 incubator.

For cell viability assays, cells were seeded in 96-well plates in triplicate at densities of 1×10^3 cells/well for the A549 cell line or 1×10^4 cells/well for the NCI-H358 cell line. After 24 hours of incubation, cells were treated with sotorasib (AMG 510; MCE, cat. HY-114277), the first FDA-approved *KRAS* G12C-specific inhibitor, at different concentrations based on their *KRAS* mutation status. NCI-H358 cells harboring the *KRAS* G12C mutation were treated with low concentrations of sotorasib (0, 0.01, 0.02, and 0.03 μM) due to their sensitivity to this G12C-specific inhibitor. In contrast, A549 cells carrying the *KRAS* G12S mutation required higher concentrations (0, 5, 15, and 25 μM) to achieve growth inhibition. Cell viability was assessed after 3 days of drug treatment using the Cell Counting Kit-8 (CCK-8, Dojindo, cat. CK04) according to the manufacturer's instructions. Absorbance was measured at 450 nm using a Synergy HTX microplate reader (BioTek).

Based on the cell viability results, sotorasib concentrations that maintained approximately 80% cell viability (as indicated by red dotted lines in Fig. 4A) were selected for subsequent experiments. Cells were seeded in 6-well plates at densities of 2×10^5 cells/well (NCI-H358) or 5×10^4 cells/well (A549). NCI-H358 cells were treated with sotorasib at 0.01 μM only, while A549 cells were treated at both 0.01 μM and 15 μM. Cells were monitored for 3 days prior to RNA extraction.

RNA extraction and cDNA synthesis

Total RNA was extracted using Trizol reagent according to the manufacturer's protocol. cDNA was synthesized using the Supe-

rScript III First-Strand Synthesis SuperMix for qRT-PCR kit (Invitrogen, cat. 11752-050) following the manufacturer's instructions.

Real-time PCR analysis

Quantitative PCR was performed using THUNDERBIRD™ SYBR qPCR Mix. The following primer sets were used: 1. *RPS24* Total Expression Analysis: Primers spanning exons 4-6 were designed to detect all AS isoforms for total gene expression quantification: Forward: 5′-ATGGCCTGTATGAGAAGAAA-3′, Reverse: 5′-CACA GCTAACATCATTGCAG-3′ (as described in (20)). 2. *RPS24* AS Isoform-Specific Detection To analyze specific AS events, the following primer sets were used: For exon 4:3bp, Forward: 5′-TGGCAAAAAGAAGTGAGCTG-3′, Reverse: 5′-AATGTTCTTGCGA AAAATCCA-3′, For exon 4:22bp, Forward: 5′-GACTTGCAAGA CATGGCCTGT-3′, Reverse: 5′-TCCAGCTCACTTTTTGCCAG-3′ (as described in (12)). For ex4:ex6, Forward: 5′-GACTTGCAAGACA TGGCCTGT-3′, Reverse: 5′-TCCTTCGGCTTTTTGCCA-3′ (as described in (12)). Relative expression of each isoform was calculated using the delta Ct (threshold cycle) method, with total *RPS24* expression used as the reference.

Fragment analysis

For fragment analysis of *RPS24* AS isoforms, PCR was performed using a fluorescein (6-FAM)-labeled forward primer and an unlabeled reverse primer spanning the region between exon 4 and exon 6, as previously described. PCR products were diluted 1:100 and subjected to capillary electrophoresis using POP-7™ Polymer (Thermo Fisher, cat. 4393708). The size and peak area of each isoform were analyzed using Peak Scanner software (Thermo Fisher Scientific). The relative abundance of each *RPS24* AS isoform was quantified by calculating the ratio of its individual peak area to the sum of all isoform peak areas.

ACKNOWLEDGEMENTS

This research was supported by the Basic Science Research Program through the National Research Foundation (NRF), funded by the Ministry of Education (RS-2022-NR075158, RS-2022-00165497, and 2019R1A5A2027588). It was also supported by KREONET (Korea Research Environment Open NETwork), which is managed and operated by KISTI (Korea Institute of Science and Technology Information), and by the Basic Medical Science Facilitation Program through the Catholic Medical Center of the Catholic University of Korea, funded by the Catholic Education Foundation.

CONFLICTS OF INTEREST

The authors have no conflicting interests.

REFERENCES

1. Kahles A, Lehmann KV, Toussaint NC et al (2018) Comprehensive analysis of alternative splicing across tumors from 8,705 patients. Cancer Cell 34, 211-224.e216
2. Tao Y, Zhang Q, Wang H, Yang X and Mu H (2024) Alternative splicing and related RNA binding proteins in human health and disease. Signal Transduct Target Ther 9, 26
3. Gonzalez-Rodriguez P, Klionsky DJ and Joseph B (2022) Autophagy regulation by RNA alternative splicing and implications in human diseases. Nat Commun 13, 2735
4. Liu J, Lin CX, Zhang X et al (2023) Computational approaches for detecting disease-associated alternative splicing events. Brief Bioinform 24, bbad106
5. Cancer Genome Atlas Research N (2014) Comprehensive molecular profiling of lung adenocarcinoma. Nature 511, 543-550
6. Huang L, Guo Z, Wang F and Fu L (2021) *KRAS* mutation: from undruggable to druggable in cancer. Signal Transduct Target Ther 6, 386
7. Cox AD and Der CJ (2025) "Undruggable *KRAS*": druggable after all. Genes Dev 39, 132-162
8. Hofmann MH, Gerlach D, Misale S, Petronczki M and Kraut N (2022) Expanding the reach of precision oncology by drugging all *KRAS* mutants. Cancer Discov 12, 924-937
9. Awad MM, Liu S, Rybkin II et al (2021) Acquired resistance to *KRAS* (G12C) inhibition in cancer. N Engl J Med 384, 2382-2393
10. Olivieri JE, Dehghannasiri R, Wang PL et al (2021) RNA splicing programs define tissue compartments and cell types at single-cell resolution. Elife 10, e70692
11. Kerry J, Specker EJ, Mizzoni M et al (2024) Autophagy-dependent alternative splicing of ribosomal protein S24 produces a more stable isoform that aids in hypoxic cell survival. FEBS Lett 598, 503-520
12. Brumwell A, Fell L, Obress L and Uniacke J (2020) Hypoxia influences polysome distribution of human ribosomal protein S12 and alternative splicing of ribosomal protein mRNAs. RNA 26, 361-371
13. Park J, Nam DH, Kim D and Chung YJ (2024) *RPS24* alternative splicing is a marker of cancer progression and epithelial-mesenchymal transition. Sci Rep 14, 13246
14. Seiler M, Peng S, Agrawal AA et al (2018) Somatic mutational landscape of splicing factor genes and their functional consequences across 33 cancer types. Cell Rep 23, 282-296.e284
15. Yan Y, Ren Y, Bao Y and Wang Y (2023) RNA splicing alterations in lung cancer pathogenesis and therapy. Cancer Pathog Ther 1, 272-283
16. Dobin A, Davis CA, Schlesinger F et al (2013) STAR: ultrafast universal RNA-seq aligner. Bioinformatics 29, 15-21
17. Putri GH, Anders S, Pyl PT, Pimanda JE and Zanini F (2022) Analysing high-throughput sequencing data in Python with HTSeq 2.0. Bioinformatics 38, 2943-2945
18. Robinson MD, McCarthy DJ and Smyth GK (2010) edgeR: a Bioconductor package for differential expression analysis of digital gene expression data. Bioinformatics 26, 139-140
19. Subramanian A, Tamayo P, Mootha VK et al (2005) Gene set enrichment analysis: a knowledge-based approach for interpreting genome-wide expression profiles. Proc Natl Acad Sci U S A 102, 15545-15550
20. Jun Y, Suh YS, Park S et al (2022) Comprehensive analysis of alternative splicing in gastric cancer identifies epithelial-mesenchymal transition subtypes associated with survival. Cancer Res 82, 543-555